An 1 H NMR Microimaging Study of Water Vapor Sorption by Individual Porous Pellets

ARTICLE *in* THE JOURNAL OF PHYSICAL CHEMISTRY B · MARCH 2000

Impact Factor: 3.3 · DOI: 10.1021/jp9922763

An ^{1}H NMR Microimaging Study of Water Vapor Sorption by Individual Porous Pellets

Igor V. Koptyug,*,† Ludmila Yu. Khitrina,‡ Yurii I. Aristov,‡ Mikhail M. Tokarev,‡ Kazizat T. Iskakov,§ Valentin N. Parmon,‡ and Renad Z. Sagdeev†

International Tomography Center, Institutskaya str. 3A, Novosibirsk 630090, Russia, Boreskov Institute of Catalysis, Acad. Lavrentiev pr. 5, Novosibirsk 630090, Russia, and Karaganda State University, Universitetskaya str. 28, Karaganda 470012, Kazakhstan

Received: July 2, 1999; In Final Form: October 15, 1999

The ^{1}H NMR microimaging technique is applied to study water vapor sorption by the individual cylindrical silica gel and alumina pellets impregnated with hygroscopic salts. The two-dimensional images or the one-dimensional profiles of the sorbed water distribution are detected sequentially to monitor the transport of water within the pellets in real time in the course of the sorption process. The results identify the propagation of the sorbed water front through the dry regions of the pellets as the rate-limiting stage of the sorption process. This propagation can be facilitated by employing the pellets with the eggshell distribution of the salt, but in such cases the salt redistributes readily in the course of the sorption process, as revealed by the relaxation weighted ^{1}H NMR microimaging experiments in which paramagnetic salts are used. The diffusion equation with water content dependent diffusivity is employed to model the one-dimensional radial profiles of water distribution within the pellet with appropriate correction for the relaxation weighting effects.

Introduction

In many industrial applications, beds of moisture adsorbing grains such as zeolites, alumina, or silica gel pellets, etc., are employed to remove moisture from a gas stream. The shape and propagation velocity of the front of the sorbed liquid which travels from the inlet toward the outlet of the absorber during its operation determine how much water can be sorbed before the tail of the front reaches the outlet. While the models which are usually employed to describe the mass transport processes in the absorbing beds assume that the bed represents a quasihomogeneous absorbing medium, in reality the bed is comprised of a large number of individual porous grains. Therefore, moisture transport within the individual grains constituting the bed is one of the important factors which affect the propagation of liquid through the bed. Hence, the progress in the design of more efficient absorbers and accurate modeling of their operation should rely on a better understanding of the mass transport processes within the individual grains.

It has been demonstrated recently[1−3] that the water vapor sorption efficiency of the porous alumina or silica gel pellets can be significantly increased by impregnating the pellets with a hygroscopic salt (e.g., $CaCl_2$, $MgCl_2$, LiBr, etc.). In the long run we are interested in identifying the possible rate-limiting stages of mass transport during the sorption process and elucidating the interplay between the pellet characteristics (pellet composition and texture, distribution of the salt within the pellet, and its redistribution upon repetitive sorption/desorption cycles, etc.) and the liquid transport efficiency. The purpose of this work was to study the transport of water within the individual porous pellets (alumina, silica gel) impregnated with the hygroscopic salts ($CaCl_2$, $CuCl_2$).

NMR microimaging has proven to be a useful tool for a nondestructive determination of spatial and temporal variations of liquid contents in a variety of porous materials, rapid enough to follow the drying[4−13] and the sorption processes[14−22] in real time. In the previous work,[23] we have successfully employed the one-dimensional (1D) NMR microimaging to obtain the radial distribution of water in porous alumina and titania cylindrical pellets during their drying. We have demonstrated that the magnitude of the 1D spin echo profiles was not an immediate measure of the water content in the sample due to the relaxation-weighting of the NMR signal. A dedicated calibration procedure has been developed[23] which yielded an empirical relation between the profile magnitude and the actual water content and allowed us to obtain quantitative characteristics of liquids transport.[24] Here, the 1D approach developed in our previous studies and the 2D microimaging are utilized to study the single pellet sorption process.

Experimental Section

Distilled water, "purum" grade cyclohexane and copper chloride, and commercial calcium chloride were used in the experiments. The texture characteristics of the silica gel and two types of γ-Al_2O_3 pellets used are given in Table 1. Depending on the desired distribution of the salt within the pellet, the following sample preparation procedures were used. The alumina or silica gel pellets were initially fully saturated with water (for the uniform salt distribution) or partially saturated with cyclohexane (for the eggshell distribution). The pellets were then placed in a saturated aqueous solution of $CaCl_2$ for several hours and then dried at 130 °C. A different procedure for obtaining the eggshell distribution consisted of wrapping an absorbing tissue presoaked with the aqueous solution of $CaCl_2$ around a dry alumina pellet. The latter approach apparently gives a lower $CaCl_2$ concentration in the "shell", and therefore is less efficient. Similar procedures were used to impregnate alumina pellets with $CuCl_2$.

* Corresponding author. E-mail: koptyug@tomo.nsc.ru. Fax: +7 3832 331399.
† International Tomography Center.
‡ Boreskov Institute of Catalysis.
§ Karaganda State University.

10.1021/jp9922763 CCC: $19.00
Published on Web 02/03/2000

TABLE 1: Specific Surface Area (A), Pore Volume (V_{pore}), and Average Pore Radius (r_{av}) of the Porous Pellets Studied in This Work

sample	A m^2/g[a]	V_{pore} cm^3/g[b] (∅ < 1500 Å)	V_{pore} cm^3/g[c] (∅ > 1500 Å)	r_{av} Å[d] (∅ < 1500 Å)	r_{av} Å[c] (∅ > 1500 Å)
silica gel	350	1.0		75	
alumina I	134	0.31	0.09	43	2500
alumina II	180	0.43	0.1	40	4000

[a] BET nitrogen adsorption method. [b] Nitrogen adsorption saturation at relative nitrogen vapor pressure $P/P_s = 0.95$, where P_s is the saturated vapor pressure at ca. 77 K. [c] Mercury porosimetry. [d] Desorption branch of nitrogen adsorption isotherm.

SCHEME 1: Sample Positioning in the Imaging Experiment

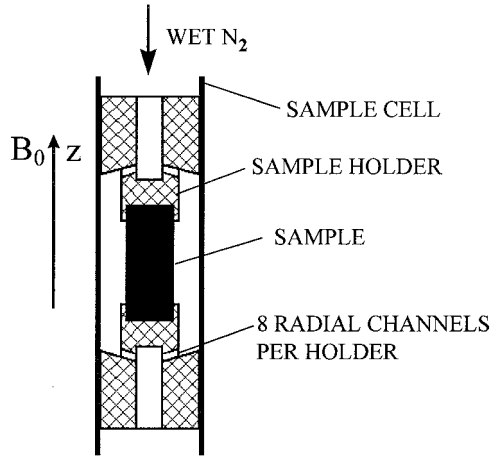

The ^{1}H NMR microimaging experiments were performed at 300 MHz on a Bruker Avance NMR spectrometer equipped with the microimaging accessory. A cylindrical alumina (∅ 3.6 mm) or silica gel (∅ 6 mm) pellet was positioned in the cylindrical glass cell (inner diameter 9.1 or 21 mm, respectively) residing in the probe of the NMR instrument. Both the sample and the cell axes were oriented along the main magnetic field of the superconducting magnet (Scheme 1). The two ends of the cylindrical sample were covered to ensure radial mass transport during the moisture sorption process. A stream of room-temperature air or nitrogen gas was first passing through a bubbler thermostated at 20 °C, and then along the pellet surface in the direction coinciding with the pellet axis. The bubbler contained a saturated aqueous solution of $CaCl_2$, $Mg(NO_3)_2$, or pure water depending on the required relative humidity of the gas (32%, 55%, or 100%, respectively). A float-type rotameter was used to measure the gas flow rate, with the typical values being 310−390 L/h.

One-dimensional concentration profiles of the sorbed water along the diameter of the cylinder with spatial resolution of 73 μm were detected employing the 1D pulse sequence described in detail earlier.[23] It starts with a projection presaturation[25] module for slice selection along the cylindrical sample axis direction (z) by destroying the magnetization outside a 5 mm thick slice in the central part of the pellet. Then a spin−echo pulse sequence {90° (soft)−180° (hard)−echo} with appropriate gradients for selection of a slice ca. 400 μm wide perpendicular to the y axis in the central part of the cylinder and frequency encoding the signal along the diametrical slab (x axis) is applied. The effective echo time was estimated as 1.9 ms. Usually 128 complex points were digitized at a highest available sampling rate corresponding to the spectral width of 125 kHz, and 32−128 phase-cycled echo signals were accumulated within 35−40 s and co-added to yield a single averaged echo. The recycling delay between successive repetitions of the pulse sequence (250 ms to 1.2 s depending on the sample) was at least $4T_1$. A complex Fourier transformation of the echo signal without zero-filling and calculation of the magnitude spectrum yielded the profile reflecting the signal intensity variation along the diameter of the cylindrical sample. Up to 256 averaged profiles were detected sequentially with ca. 40 s interval to monitor the sorption process in real time. Further experimental details of the 1D microimaging experiment can be found elsewhere.[23]

For the 2D visualization of water vapor sorption by a silica gel pellet, the single point imaging (SPI) technique was employed.[7,26−29] The square field of view (FOV) was 1 cm^2 with a square data matrix of 64 × 64 data points. The repetition time was $T_R = 200$ ms, the phase encoding time was $T_P = 400$ μs. Because of a rather long excitation pulse employed (70 μs), the actual resolution of the image is expected to be lower than the nominal one. Acquisition of each 2D SPI image required 13 min 39 s.

For 2D visualization of the redistribution of $CuCl_2$, a slice-selective spin−echo sequence with the echo time $T_E = 3.2$ ms and a varying repetition time T_R (0.15−1.5 s) was used. The slice imaged was 4 mm thick in the center of the sample perpendicular to the cylinder axis. The data matrix contained 128 × 128 data points and covered a square FOV of 1 cm^2. The results of the four phase-cycled repetitions of the experiment were averaged for the artifact and noise reduction. The alumina pellet containing $CuCl_2$ was imaged before the first sorption cycle and after several successive sorption cycles. Each time before the experiment the water was removed by drying at 130 °C and the pellet was saturated with cyclohexane and imaged. The pellet was then dried again to remove cyclohexane and used in the next water sorption experiment. Cyclohexane was used for the visualization of the salt to ensure that due to the low solubility of $CuCl_2$ in cyclohexane no salt redistribution occurs between the sorption cycles while the images are obtained. Besides, the somewhat longer T_2 times of cyclohexane in alumina pellets as compared to those of water facilitate the application of spin−echo sequence.

Results and Discussion

Figure 1a visualizes the water vapor sorption process by a cylindrical silica gel pellet (∅ 6 mm) with a uniform distribution of $CaCl_2$. The 2D projections onto the plane perpendicular to the cylinder axis are shown in the figure. The accumulation time for each projection was ca. 820 s, which means that each projection is not an instantaneous "snapshot" of the water distribution in the pellet, but rather represents a distribution averaged over a substantial period of time. Nevertheless, for the pellets of a relatively large diameter the 2D approach provides a fairly accurate visualization of the sorption process. For smaller pellets (∅ 1−3 mm) often used in practical applications, the 2D approach becomes prohibitively slow, since in that case it takes much less time to fill out the entire pellet with water.

The useful information provided by the 2D imaging experiment is that the results demonstrate a nearly perfect cylindrical symmetry of the process despite the possible presence of the local defects in the pellet and possible spatial variations in the gas flow due to the influence of the sample holders. Therefore, a one-dimensional radial profile of water content is sufficient to fully characterize the distribution of water within the pellet. The 1D profiles of water content along the diameter of the cylindrical pellet for the same silica gel sample under similar

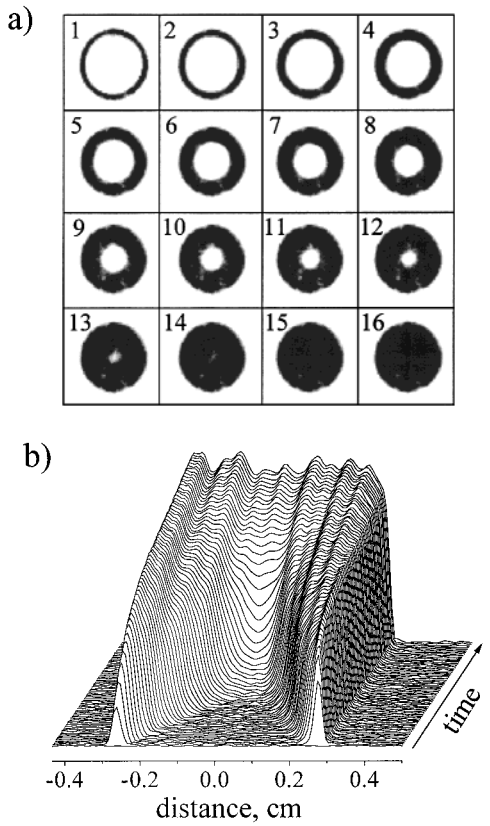

Figure 1. Visualization of the dynamics of the water sorption by a cylindrical silica gel pellet containing $CaCl_2$ with uniform distribution of the salt. Air flow FL = 390 L/h; relative air humidity RH = 55%. (a) 2D SPI images; accumulation time per image was 13 min 39 s. (b) 1D profiles of water content along the diameter of the pellet, accumulation of each profile lasted 34 s, every 8th profile is shown. The overall time span of the experiment was 290 min.

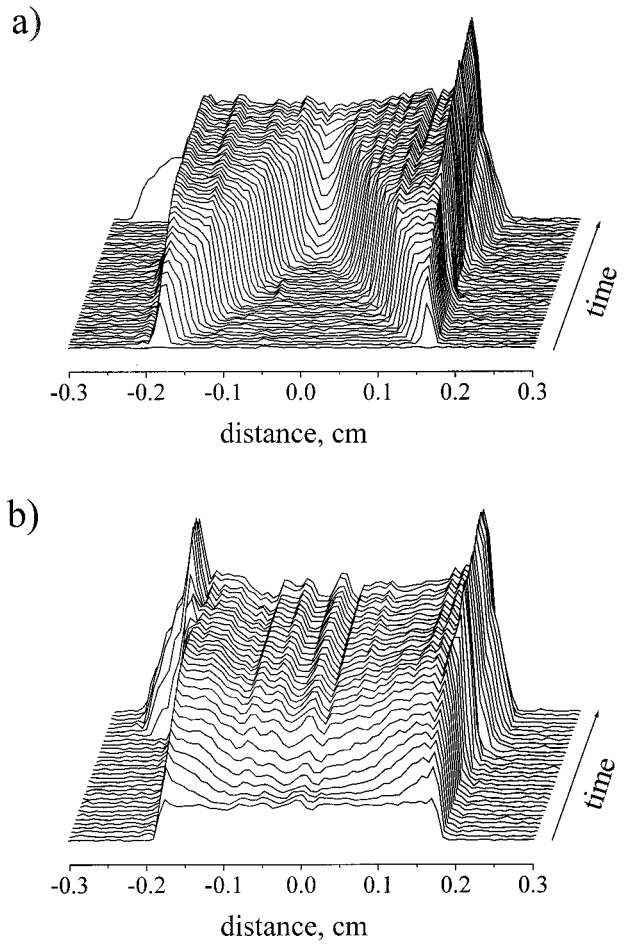

Figure 2. 1D water content profiles detected in the course of the water sorption by a cylindrical alumina pellet with uniform distribution of $CaCl_2$. Accumulation time of each profile was 38.5 s, every other profile is shown; FL = 310 L/h, RH = 100%. The initial water contents of the pellet were (a) 0% and (b) 56%. The overall time span of the experiment was (a) 58 and (b) 41 min.

conditions are shown in Figure 1b. It takes much less time to acquire a 1D profile (ca. 35 s) as compared to a 2D one; therefore, the 1D profile is a better representation of an instantaneous distribution of water at a given time. Besides, the process of water sorption by the smaller pellets can be studied.

Parts a and b of Figure 2 demonstrate that the 1D approach can be successfully employed to study sorption by the smaller pellets (∅ 3.6 mm) and can yield the important details regarding the mass transport within these pellets. Figure 2a shows the results obtained for an initially dry alumina pellet with a uniform distribution of $CaCl_2$. As can be seen from the figure, the rate of water transport is limited by the penetration of liquid into the dry regions of the pellet, and the propagation of the sorbed water in this case is characterized by a sharp front. This behavior resembles the non-Fickian (case II) transport of solvents upon their uptake by polymers.[30−35] In fact, the analogy can have a solid physical background. For the observation of the case II transport behavior it is essential that the liquid penetrating into the dry glassy network induces the glass-to-rubber transition of the polymer, whereas if the polymer is in a rubbery (or glassy) state throughout the entire uptake process, the behavior is Fickian.[30] In our case, the transition is brought about by the dissolution of the solid $CaCl_2$ upon water uptake.

Figure 2b demonstrates that the propagation of the water front through the pellet partially saturated with water is indeed different. The results depicted in Figure 2b were obtained for the same pellet as in Figure 2a, but with an initial uniform water saturation of 56%. (Note that due to the relaxation weighting effects the intensity of the initial profile in Figure 2b is only 27% of the profile corresponding to the pellet fully saturated with water). The Fickian ingress of water into the pellet in the latter case is obvious, indicating that liquid transport at such saturations is more efficient than that through a dry pellet. The analogy of the process under study with the solvent ingress into polymers is interesting and opens up the possibility of employing the mathematical models developed for the latter process to the description of the water sorption. This possibility will be explored further in the future work.

The results of our earlier studies of drying of the alumina pellets have shown that capillary diffusion in unmodified alumina pellets is very efficient and is characterized by the diffusivity values which at large saturations exceed the water self-diffusion coefficient.[24] It is therefore reasonable to expect that the ingress of water into an alumina matrix which does not contain any salt should be faster than that for a similar pellet containing $CaCl_2$. However, unmodified alumina is much less efficient in adsorbing moisture. A compromise consists of preparing an alumina pellet with an eggshell distribution of $CaCl_2$. The adsorbing ability of such a pellet is not expected to be significantly impaired, since, as it can be seen from Figure 2a, shortly after the initiation of the sorption process the volume adjacent to the surface of the pellet becomes almost fully saturated with water, and the inner regions do not contribute significantly to the efficiency of sorption, while the entire process is rate-limited by the liquid transport into the inner parts

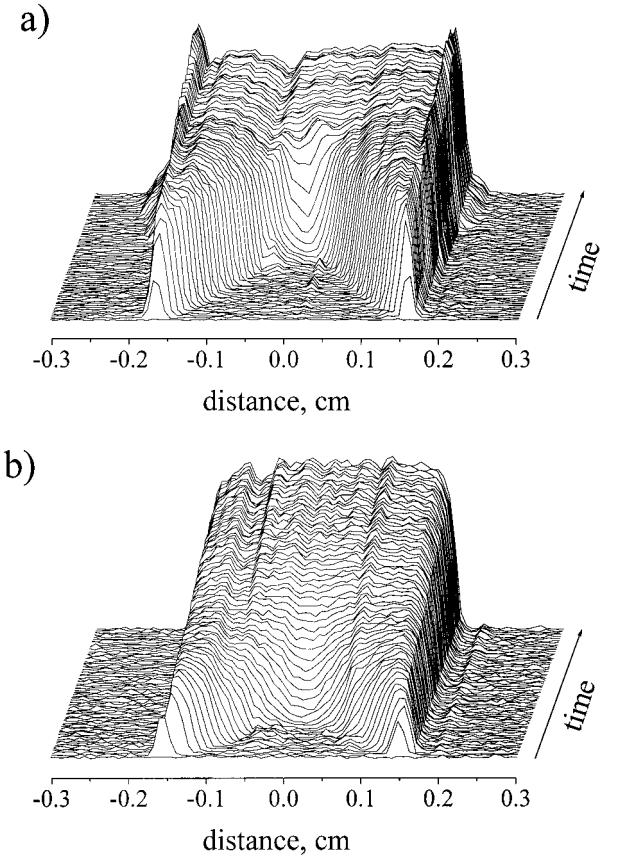

Figure 3. 1D water content profiles detected in the course of the water sorption by an initially dry cylindrical alumina pellet. Accumulation time of each profile was 38.5 s, every 4th profile is shown; FL = 370 L/h, RH = 55%. The results for (a) uniform and (b) eggshell distribution of $CaCl_2$ are compared. The overall time span of each experiment was 164 min.

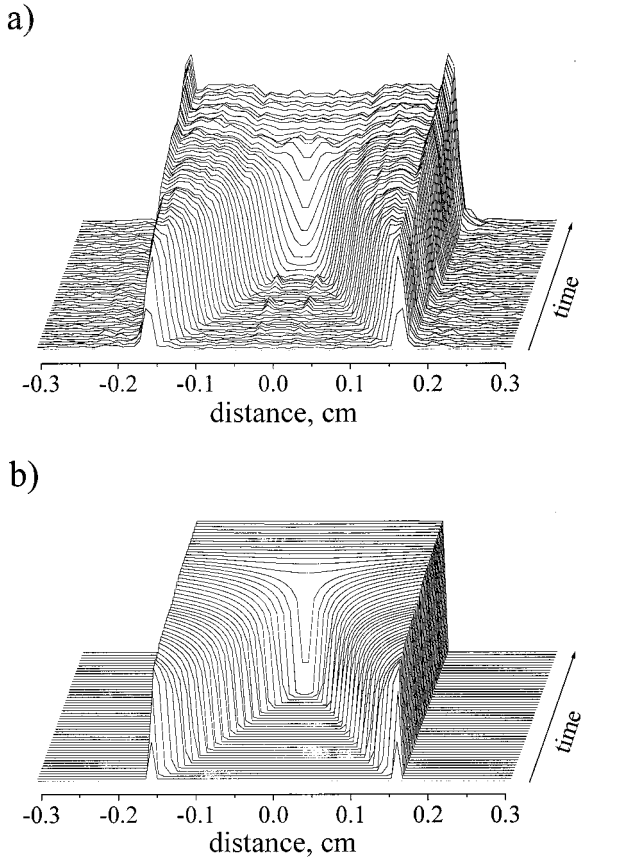

Figure 4. Water sorption by an alumina pellet with uniform distribution of $CaCl_2$: (a) experimental and (b) simulated 1D water content profiles. The experimental parameters are the same as in Figure 3a, except the time span which was reduced to 128 min.

of the pellet. On the other hand, the eggshell distribution of $CaCl_2$ is expected to facilitate water transport once the water reaches the inner salt-free part of the pellet. Figure 3 demonstrates that this approach can indeed make the water transport faster. An obvious difference in the water front propagation between the uniform and the eggshell distributions of $CaCl_2$ is observed.

While the qualitative comparison of the transport for the two types of salt distribution is informative, it would be useful to have a (semi)quantitative parameter characterizing the process under study. A relatively simple model which nevertheless can provide a reasonable description of the mass transport process is based on the solution of the diffusion equation with water content dependent diffusivity. We have previously demonstrated that it can be successfully employed to describe water transport observed in the course of the alumina pellet drying.[24,36] In this work, we employed basically the same approach as in the previous studies,[24,36] but with two essential modifications. First, we reformulated the radial diffusion equation in terms of the observed signal intensity (S) rather than the actual water content (C):

$$\frac{dC}{dS}\frac{\partial S}{\partial t} = \frac{1}{r}\frac{\partial}{\partial r}\left(rD(C)\frac{dC}{dS}\frac{\partial S}{\partial r}\right) \qquad (1)$$

The required relation $S = S(C)$ is obtained in the calibration experiment described earlier.[23] Second, instead of the flux at the external surface, we used the measured signal intensity as the boundary condition at the sample surface. It is assumed that the dependence of the diffusivity on the actual water content is of the form

$$D(C) = D_e \exp(-\gamma(1 - C/C_0)) \qquad (2)$$

where C_0 is the water content of a fully saturated pellet. The values of D_e and γ are treated as variable parameters. The finite difference scheme employed to numerically solve eq 1 is analogous to that employed earlier.[24,36] It will be described in detail elsewhere.

The results of simulations are shown in Figures 4 and 5. Because of the simplicity of the model, not all of the details of the profiles transformations are reproduced. Nevertheless, the agreement between the experiment and the calculation is acceptable, and the differences between the uniform and eggshell salt distribution are reproduced quite well. The optimized $D(C)$ dependencies are plotted in Figure 6 in the logarithmic scale. The Figure demonstrates that at 50% saturation the diffusivity for the pellet with the eggshell salt distribution exceeds that of the pellet with the uniform distribution by more than 2 orders of magnitude, and at zero saturation the difference amounts to 5 orders of magnitude. Of course, the significance of the diffusivity values obtained in these simulations should not be overestimated. A different type for the $D(C)$ dependence would give somewhat different numerical values for the diffusivity. Besides, it is likely that the diffusivity depends on the temperature and will vary during the experiment due to the exothermic nature of the sorption process. Yet another possible complication is the process of salt dissolution upon water uptake. Indeed, the data sets of parts a and b of Figure 2 cannot be modeled using the same values of D_e and γ. However, the results

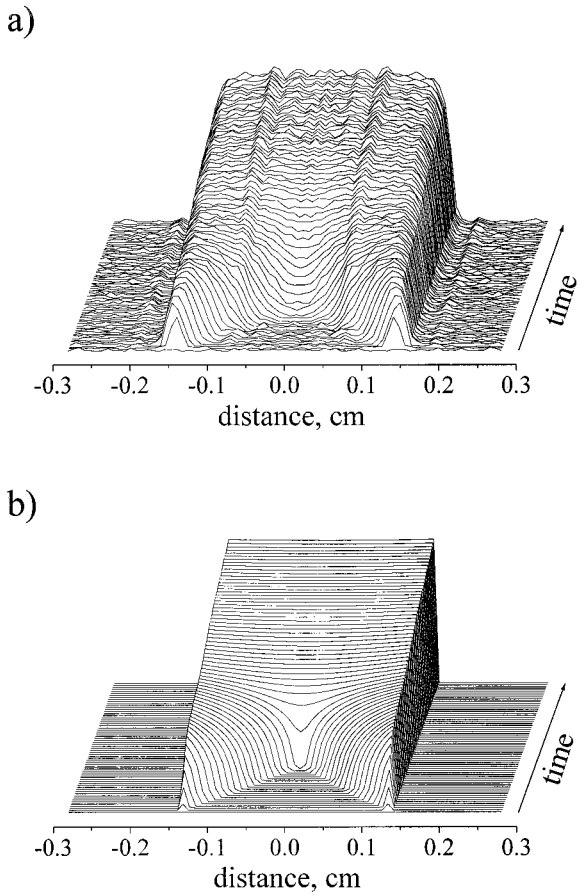

Figure 5. Water sorption by an alumina pellet with eggshell distribution of $CaCl_2$: (a) experimental and (b) simulated 1D water content profiles. The experimental parameters are the same as in Figure 3b.

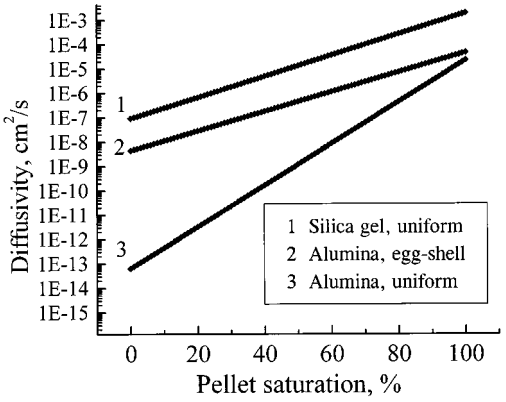

Figure 6. Optimized exponential $D(C)$ dependencies (eq 2) for water transport during the sorption for the silica gel pellet with uniform distribution of $CaCl_2$ (line 1) and the alumina pellets with eggshell (2) and uniform (3) salt distributions.

described above demonstrate that any realistic model would yield significantly larger diffusivity values for the pellet with the eggshell salt distribution.

Interestingly, the transport of water in the silica gel pellet with uniform distribution of $CaCl_2$ is more efficient than that for the alumina pellet with the eggshell distribution of $CaCl_2$. This can be attributed to the different sample composition and texture (cf. Table 1). The diffusivity values obtained by modeling the results of Figure 1b are also shown in Figure 6.

An important parameter for the eggshell type pellets is the thickness of the $CaCl_2$ "shell". The influence of this factor on the efficiency of sorption by a porous pellet has to be studied

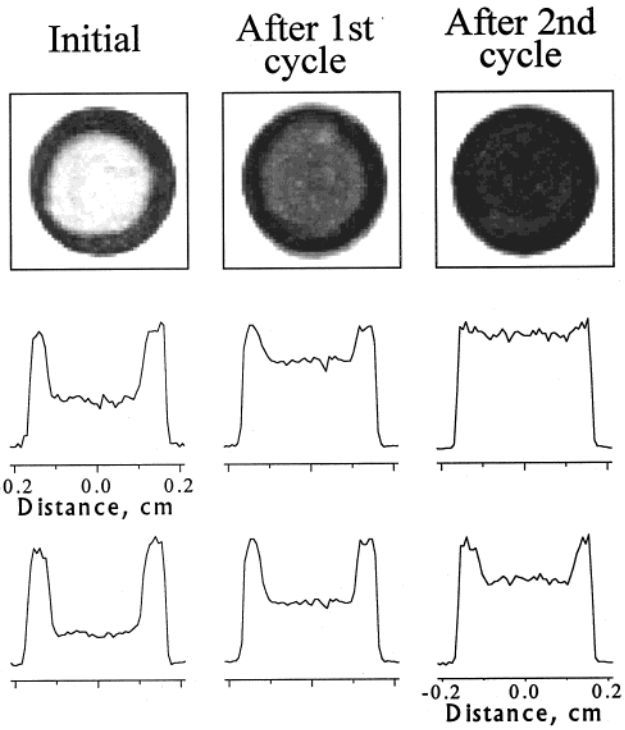

Figure 7. Spin-lattice relaxation time (T_1) weighted images of cyclohexane in the alumina pellet containing $CuCl_2$. Regions with larger salt contents give stronger signal in the image. The images show the initial eggshell distribution of $CuCl_2$ (left column) and its redistribution after one (middle) and two (right column) water sorption cycles. Two-dimensional images detected with repetition time $T_R = 1.5$ s (top row) and their one-dimensional cross sections through the pellet center (middle row), as well as the cross sections of the images detected with $T_R = 0.8$ s (bottom row) are presented.

further. To make this feasible, however, it is necessary to develop a reliable procedure for the preparation of the pellets with a known amount of the salt forming a shell of a known thickness. Further limitation of this approach is posed by the redistribution of the salt within the pellet upon multiple sorption/desorption cycles unless it is bound (e.g., chemically) to the pore walls. To demonstrate that such redistribution is likely to occur, we used the ability of ^1H NMR microimaging to indirectly map the local amounts of paramagnetic substances via the nuclear spin relaxation enhancement of the protons of liquids brought in contact with paramagnetic species. Copper chloride was used instead of $CaCl_2$, and an alumina pellet with an initial eggshell distribution of $CuCl_2$ was prepared and used in the repetitive sorption/drying experiments. Figure 7 clearly demonstrates that while the overall eggshell character of the salt distribution remains unchanged, there is an increase in the $CuCl_2$ content in the inner part of the pellet after the water sorption cycles, as indicated by a faster relaxation (stronger signal on T_1-weighted images) of cyclohexane protons.

A similar, and probably even more substantial redistribution of salt can be expected for the $CaCl_2$. This results in a lower salt content in the "shell", and in a decrease of the sorption rate. This is confirmed by Figure 8, which shows the temporal behavior of the pellet saturation with water for two alumina pellets, one with uniform and another with the eggshell distribution of $CaCl_2$. The water uptake by the alumina pellet with the eggshell distribution is somewhat faster at early times, but later this pellet becomes less efficient in sorbing water despite a substantially faster transport within the pellet volume. Therefore, the immobilization (e.g., by chemical bonding) of

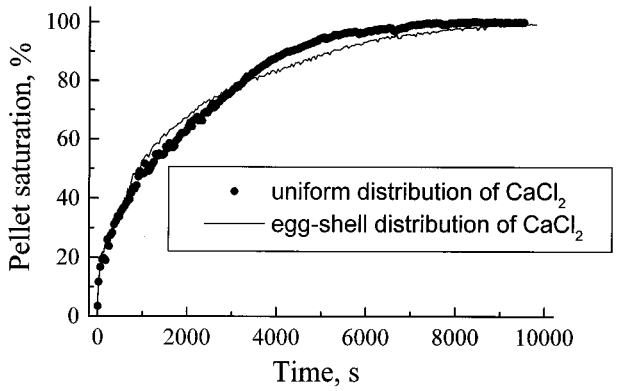

Figure 8. Temporal variation of the total amount of water in the alumina pellets with uniform and eggshell distributions of $CaCl_2$ in the course of the sorption process. The curves are derived from the sets of 1D profiles shown in Figure 3a,b with appropriate correction for relaxation weighting effects.

the salt is essential for the design of more efficient adsorbing pellets with nonuniform salt distributions.

Conclusions

By applying the ^1H NMR microimaging technique we have established the basic features of water transport within the individual porous pellets containing $CaCl_2$ upon water vapor sorption. The experimental results demonstrate that soon after the initiation of the sorption process the regions of the pellet adjacent to the surface become fully saturated with water and therefore the salt in the inner parts of the pellet does not contribute to the sorption efficiency. Furthermore, due to the presence of the salt in the inner regions of the pellet, the penetration of water into the dry areas becomes the bottleneck of the sorption process. This is confirmed by the experiments with an eggshell distribution of the salt in the pellet, in which case the inner-region transport becomes more efficient. Such distribution, however, is impractical due to the salt redistribution processes upon repetitive sorption/desorption cycles, unless one finds a way to immobilize the salt by, e.g., chemically binding it to the matrix.

The simulations of the experimental water content profiles have been carried out on the basis of the diffusion equation with the water content dependent diffusivity. The results of these simulations confirm that the diffusivity values can be several orders of magnitude larger for the eggshell distribution of $CaCl_2$ in alumina pellets as compared to the same pellets with uniform salt distribution. Of the two types of pellets studied in this work, the silica gel pellets demonstrate much larger effective diffusivity as compared to the alumina pellets, yet the rate of sorption is still limited by the liquid penetration into the pellet, as evidenced by a rapid saturation of the surface regions and a sharp front propagating at a constant velocity. The results obtained imply that any realistic model of mass transport within the beds of absorbing grains will have to explicitly account for the mass transport within the individual grains rather than treat the bed as a quasihomogeneous medium.

Acknowledgment. We thank the Russian Foundation for Basic Research (Projects 99-03-32314a and 99-03-32312a) and the Siberian Division of the Russian Academy of Sciences for financial support of this work. L. Yu. Khitrina gratefully acknowledges a scholarship awarded by the Zamaraev International Charitable Scientific Foundation.

References and Notes

(1) Aristov, Yu. I.; Tokarev, M. M.; Cacciola, G.; Restuccia, G. *React. Kinet. Catal. Lett.* **1996**, *59*, 325−328.
(2) Tokarev, M. M.; Aristov, Yu. I. *React. Kinet. Catal. Lett.* **1997**, *62*, 143−150.
(3) Gordeeva, L. G.; Restuccia, G.; Cacciola, G.; Aristov, Yu. I. *React. Kinet. Catal. Lett.* **1998**, *63*, 81−88.
(4) Hollewand, M. P.; Gladden, L. F. *Magn. Reson. Imaging* **1994**, *12*, 291−294.
(5) Hughes, P. D. M.; McDonald, P. J.; Rhodes, N. P.; Rockliffe, J. W.; Smith, E. G.; Wills, J. *J. Colloid Interface Sci.* **1996**, *177*, 208−213.
(6) Guillot, G.; Trokiner, A.; Darrasse, L.; Saint-Jalmes, H. *J. Phys. D: Appl. Phys.* **1989**, *22*, 1646−1649.
(7) Bogdan, M.; Balcom, B. J.; Bremner, T. W.; Armstrong, R. L. *J. Magn. Reson. A* **1995**, *116*, 266−269.
(8) Beyea, S. D.; Balcom, B. J.; Bremner, T. W.; Prado, P. J.; Green, D. P.; Armstrong, R. L.; Grattan-Bellew, P. E. *Cem. Concr. Res.* **1998**, *28*, 453−463.
(9) Pel, L.; Brocken, H.; Kopinga, K. *Int. J. Heat Mass Transfer* **1996**, *39*, 1273−1280.
(10) Perez, E.; Kauten, R.; McCarthy, M. J. In *Drying '89*; Mujumdar, A. S., Ed.; New York: Hemisphere, 1989; pp 149−156.
(11) Olson, J. R.; Chang, S. J.; Wang, P. C. *Can. J. For. Res.* **1990**, *20*, 586−591.
(12) Song, H.; Morris, H. D.; Litchfield, J. B. *J. Agric. Eng. Res.* **1992**, *53*, 51−69.
(13) Ruan, R.; Schmidt, S. J.; Schmidt, A. R.; Litchfield, J. B. *J. Food Process. Eng.* **1991**, *14*, 297−313.
(14) Prado, P. J.; Balcom, B. J.; Jama, M. *J. Magn. Reson.* **1999**, *137*, 59−66.
(15) Pel, L.; Hazrati, K.; Kopinga, K.; Marchand, J. *Magn. Reson. Imaging* **1998**, *16*, 525−528.
(16) Bohris, A. J.; Goerke, U.; McDonald, P. J.; Mulheron, M.; Newling, B.; Le Page, B. *Magn. Reson. Imaging* **1998**, *16*, 455−461.
(17) Papavassiliou, G.; Milia, F.; Fardis, M.; Rumm, R.; Laganas, E.; Jarh, O.; Sepe, A.; Blinc, R.; Pintar, M. M. *J. Am. Ceram. Soc.* **1993**, *76*, 2109−2111.
(18) Black, S.; Lane, D. M.; McDonald, P. J.; Hannant, D. J.; Mulheron, M.; Hunter, G.; Jones, M. R. *J. Mater. Sci. Lett.* **1995**, *14*, 1175−1177.
(19) Kärger, J.; Seiffert, G.; Stallmach, F. *J. Magn. Reson. A* **1993**, *102*, 327−331.
(20) Kärger, J.; Pfeifer, H. *Magn. Reson. Imaging* **1994**, *12*, 235−239.
(21) Halse, M. R. *Magn. Reson. Imaging* **1996**, *14*, 745−750.
(22) Hughes, P. D. M.; McDonald, P. J.; Smith, E. G. *J. Magn. Reson. A* **1996**, *121*, 147−153.
(23) Koptyug, I. V.; Fenelonov, V. B.; Khitrina, L. Yu.; Sagdeev, R. Z.; Parmon, V. N. *J. Phys. Chem. B* **1998**, *102*, 3090−3098.
(24) Koptyug, I. V.; Kabanikhin, S. I.; Iskakov, K. T.; Fenelonov, V. B.; Khitrina, L. Yu.; Sagdeev, R. Z.; Parmon, V. N. *Chem. Eng. Sci.* **2000**, *55*, 1559−1571.
(25) Singh, S.; Deslauriers, R. *Concepts Magn. Reson.* **1995**, *7*, 1−27.
(26) Emid, S.; Creyghton, J. H. N. *Physica* **1985**, *128B*, 81−83.
(27) Gravina, S.; Cory, D. G. *J. Magn. Reson. B* **1994**, *104*, 53−61.
(28) Axelson, D. E.; Kantzas, A.; Eads, T. *Can. J. Appl. Spectrosc.* **1995**, *40*, 16−26.
(29) Choi, S.; Tang, X.; Cory, D. G. *Int. J. Imaging Syst. Technol.* **1997**, *8*, 263−276.
(30) Cody, G. D.; Botto, R. E. *Macromolecules* **1994**, *27*, 2607−2614.
(31) Cody, G. D.; Botto, R. E. *Energy Fuels* **1993**, *7*, 561−562.
(32) Valtier, M.; Tekely, P.; Kiéné, L.; Canet, D. *Macromolecules* **1995**, *28*, 4075−4079.
(33) Ercken, M.; Andriaensens, P.; Vanderzande, D.; Gelan, J. *Macromolecules* **1995**, *28*, 8541−8547.
(34) Weisenberger, L. A.; Koenig, J. L. *J. Polym. Sci. C: Polymer Lett.* **1989**, *27*, 55−57.
(35) Perry, K. L.; McDonald, P. J.; Randall, E. W.; Zick, K. *Polymer* **1994**, *35*, 2744−2748.
(36) Kabanikhin, S. I.; Koptyug, I. V.; Iskakov, K. T.; Sagdeev, R. Z. *J. Inv. Ill-Posed Problems* **1998**, *6*, 335−351.